Research Square

Preprints are preliminary reports that have not undergone peer review.
They should not be considered conclusive, used to inform clinical practice,
or referenced by the media as validated information.

Dwindling Groundwater Reserves Will Threaten Mountain Streamflow in a Warmer World

Rosemary Carroll (rosemary.carroll@dri.edu)
rosemary.carroll@dri.edu
Richard Niswonger
USGS
Craig Ulrich
LBNL
Charuleka Varadharajan
LBNL
Erica Siirila-Woodburn
Lawrence Berkeley National Laboratory https://orcid.org/0000-0001-9406-124X
Kenneth Williams
Lawrence Berkeley National Laboratory https://orcid.org/0000-0002-3568-1155

Article

Keywords:

Posted Date: November 10th, 2023

DOI: https://doi.org/10.21203/rs.3.rs-3405349/v1

License: This work is licensed under a Creative Commons Attribution 4.0 International License.
Read Full License

Additional Declarations: There is **NO** Competing Interest.

Abstract

Groundwater storage and release in mountain systems is often ignored compounding uncertainty in how these systems may respond to climate change. To assess the importance of groundwater to mountain streamflow, we combine an extensive data network with a high-resolution, integrated hydrologic model stretching into the deep subsurface for a Colorado River headwater basin. In a warmer climate, increased forest water use reduces recharge, thereby destabilizing groundwater storage such that it cannot recover to historical levels even during simulated wet periods. Groundwater depletion significantly reduces average annual streamflow and forces the basin toward non-perennial conditions during dry water years. Groundwater declines are amplified in high-relief, conifer-dominated catchments. Upscaling model results across the region indicates concentrated risk of groundwater decline in the Colorado Headwater and Gunnison Basins. Research highlights the tight coupling of topography, vegetation and groundwater dynamics and that excluding groundwater response to warming will underestimate future reductions in mountain streamflow.

INTRODUCTION

The Colorado River is a major water source and economic engine for the southwestern United States (US). Nearly 90% of its water originates from the snow-dominated watersheds in Colorado, Utah and Wyoming[1] to support 40 million people and $1.4 trillion in economic activity[2]. The Colorado River is currently grappling with a multi-decadal drought[3,4] with legal and political tensions rising to develop voluntary cuts in water use as a result of diminishing supply[5]. Declining streamflow and reservoir storage, however, cannot be explained solely by lower precipitation in its headwater basins. As an example, in 2021, the Upper Colorado River Basin (UCRB) received 80% normal snowpack but delivered only 30% of average streamflow to its receiving reservoir[6]. Accelerated warming in mountain basins may be part of the explanation[7]. Warming reduces snowpack accumulation by shifting more precipitation toward rain, enhancing mid-season melt events and increasing snow vapor losses[8]. Increased snow drought and associated snowpack declines are observed across the western US since the mid-20th century [9,10] and the UCRB is projected to move toward persistent low-to-no snow conditions over 50% of its area by the end of this century[11]. Research has indicated that changes in snowpack with warming are expected to decrease mountain streamflow through preferential partitioning of precipitation toward increased vegetation water use in the soil zone[12,13].

While effects of warming on snowpack and soil water processes have been explored, there remains considerable uncertainty on the relative importance of groundwater sourcing to mountain streamflow[14]. The prevailing assumption has been that these systems have limited groundwater storage and steep hydraulic gradients with streamflow more reliant on surface processes that control runoff and interflow, or shallow subsurface water flow through the soil and regolith[15,16]. However, there is growing evidence that groundwater contributes 10 to 50% the annual streamflow in mountain catchments of the Colorado River[17–19]. While stored groundwater release has the potential to buffer streamflow to short-term climate

extremes[20–22], how groundwater storage will respond to multi-decadal warming and how this may affect streamflow generation in mountain basins is largely unknown. Understanding groundwater flow to mountain streams is hindered by the need to quantify the interaction of climate and snow dynamics[23–26], soil water storage and loss to vegetation[27], and their combined effects on groundwater generation, or recharge[28]. Modeling these processes in mountain basins at the appropriate resolution (100–250 m[29]) is numerically expensive, while obtaining sufficient data to constrain is difficult due to challenges in site access and harsh climate[30].

To address these challenges, we focus on the East River, Colorado (750 km^2, Fig. 1a). The East River is representative of many headwater basins of the UCRB[31]. The climate is continental subarctic, and it spans nearly 2 km in vertical relief (2440–4300 m). It is home to the largest atmosphere-to-bedrock observational network in the US with investment across multiple federal agencies, national laboratories, university partners, and regional stakeholder groups[32]. Data includes airborne mapping of snowpack[33,34], vegetation[35], and bedrock resistivity[36], as well as dense arrays that monitor snowpack, groundwater, and streamflow. Data informs an integrated hydrologic model of the basin[37]. A 100-m grid resolution represents topographic complexity and a daily timestep accounts for energy and water partitioning between the snowpack, vegetation, soil zone and bedrock. Details on the land surface model construction and calibration are provided in previous work[38]. Here it is dynamically linked to a three-dimensional groundwater flow model[39] that allows for streamflow gaining and losing conditions[40]. The groundwater model accounts for nine stratigraphic units[41] and extends 400 m below land surface (Fig. 1b). Inclusion of the deep subsurface is based on the growing evidence that non-trivial groundwater flow to streams can occur at considerably greater depth than previously believed[42], even in fractured crystalline[43] and metamorphic rock[44]. Simulated depth to the water table is provided in Fig. 1c with open water indicating groundwater-fed perennial streams. Refer to the Methods and Supplemental Information for details on data sources (Table S1), historical climate and model construction (Fig. S1-S9, Table S2).

Hydrologic sensitivity to temperature is tested by applying + 4°C to historical minimum and maximum daily temperatures for water years 1987 to 2022 with no change in precipitation (water year 1 Oct to 30 Sept). This extrapolates locally observed temperature and (lack of) precipitation trends to roughly the end-of-century (Table S3). Independently, sensitivity to fall, winter, spring and summer warming is tested by applying temperature increases to only to those months defining a particular season. The experimental design allows a direct comparison to the historical baseline condition and a comparison of relative effects of season (see Methods for limitations). Using this data- modeling framework we explore historical water budgets and the relevance of groundwater sourcing to streams. We then ask how sensitive is streamflow generation in a significantly warmer climate and how and where does changing groundwater storage factor in to estimated changes in streamflow?

Conceptual model of mountain hydrology and the importance of lateral flow

To predict groundwater to streams in mountain basins it is necessary to track the entire water budget, including snow dynamics, soil moisture, evapotranspiration (ET), and lateral subsurface flow. Modeled historical conditions indicate annual precipitation (P) is high (947 ± 176 mm) and arrives primarily as snow (Fig. 2). The summer monsoon delivers approximately 20 ± 6% of annual water input and this is important for sustaining vegetation water demand in the late summer[45]. At the basin-scale, the East River is generally energy-limited such that aridity, or the ratio of potential evapotranspiration (PET) to P is less than 1.0. Despite being a wet and cold climate, simulated ET accounts for more than half the water exported out of the basin with the majority of ET derived from the soil zone. Results align with observed data[46] and fit the Budyko framework[47] such that the ratio of ET/P is tightly coupled to aridity with soil water increasingly used to support ET under drier conditions (Fig. S10). While ET sourced from groundwater (ETg) is a fairly small portion of the average annual water budget at the basin scale (2 ± 1%), it becomes increasingly important in years when aridity is relatively high, especially when summer monsoon rains fail. Despite ET/P sensitivity to interannual variation in aridity, the total ET volume is consistent year-to-year to suggest the East River is soil storage limited[48] with average annual soil moisture relatively insensitive to winter and spring precipitation that represent the bulk of water inputs to the basin. Instead, annual soil moisture is more sensitive to summer temperatures and monsoon rain (Table S4). Warm and dry conditions in the summer and fall promote dry soils that last through the winter months[49] to reduce recharge, interflow to streams and streamflow efficiency in the subsequent snowmelt season (Fig. S11).

Groundwater generation is divided into areal recharge and seepage. Areal recharge is the vertical flux of water from the soil zone into the deeper subsurface. Areal recharge is relatively low in the East River as a consequence of steep topography, limited soil storage, and permeability contrasts between the soil and underlying bedrock that preferentially partitions excess soil water toward lateral movement, or interflow. Interflow moves snowmelt downgradient towards topographic convergent zones to form streams. Stream channels that are disconnected from groundwater are non-perennial with a portion of their flow seeping back into the underlying groundwater system as a function of hydraulic head differences between the stream water surface and water table elevation. Similar to previous mountain studies[50,51], this topographic focusing of snowmelt and gradient-driven seepage loss is estimated as the dominant form of recharge. Interflow and runoff that remains in the river channel (combined Qs) represents the bulk of streamflow in the East River (74 ± 29%). Qs is highly responsive to interannual variability in aridity and plots nonlinearly as an inverse image to ET/P indicating its tight coupling to vegetation water use (refer to Fig. S10d for stream sources). Groundwater discharge to streams (Qg) is estimated at approximately 12% the total water budget and represents 26 ± 7% of total annual streamflow, though extreme wet and dry water years stretch the fraction of Qg in streamflow between 8% and 48% in response to highly variable Qs contributions. In contrast to Qs, volumetric inputs of Qg are a stable source of streamflow that are relatively insensitive to aridity. Instead, Qg responds as a direct, exponential function of groundwater storage ($r = 0.85$, $p << 0.01$) (Fig. S12).

Elevation is a first-order control in the ER, with codependent relationships between climate and vegetation that influence water storage and movement (Fig. 3). Broadly, the alpine occurs above tree line (> 3500 m), the upper subalpine is a mixture of lower density conifer forests, shrubs, and barren ground (3200–3500 m), the lower subalpine is predominantly conifer forests mixed with aspen and meadows (2800-3200m). The montane (< 2800 m) is dominated by shrubs. The transition between the upper and lower subalpine is distinguished as the transition between energy and water limitation during historically low precipitation water years and coincides with the maximum density of conifer cover[38]. Simulated snow water equivalent (SWE) is orographically controlled, but this is modified by wind and avalanche[26] to push maximum snow accumulation towards tree line[51]. The combined effect of soil evapotranspiration, sublimation, and canopy interception loss (ETa) is largest where PET = P during historically dry conditions. Under average and wet conditions maximum ETa occurs at lower elevations with the downgradient movement of excess interflow [52]. At lower elevations and years with low precipitation, groundwater subsidizes ETg.

While average annual basin-scale ET volume is relatively stationary from one year to the next, the spatial distribution of ET does vary (Fig. S13). ET increases during years with low precipitation at higher elevation as aridity approaches unity and the growing season lengthens through reductions in snow-covered area and warmer seasonal temperatures. At lower elevations, ET decreases during years with low precipitation due to water limitation. The largest decreases are along south-southwest aspects. Exceptions occur within riparian corridors where shallow water tables occur, and groundwater can support vegetation water use even under drought. Annual precipitation in excess of streamflow and ET results in a net gain in subsurface storage ($dS = P-ET-Q > 0$). This occurs primarily in the alpine and upper subalpine zones. Excess water supports both areal recharge and moves laterally through the soil zone to support downgradient streamflow and evapotranspiration in water-limited portions of the basin ($dS < 0$). Results agree with previous studies in which the lateral transfer of high elevation snow melt (and nutrients) subsidizes lower elevation carbon stocks[53], above-ground productivity[54] and vegetation[55]. Maximum streamflow generation is simulated to occur in the forested subalpine as a mixture of both Qs and Qg with the influence of groundwater on streamflow remaining stable but increasing in its relative contributions at lower elevations and during dry water years as soil water preferentially partitions away from Qs and toward vegetation water use.

Hydrologic response to a warmer climate

We compare the annual changes in hydrologic storage and their associated fluxes due to multi-decadal warming during the driest water year with its historical equivalent across different elevations (Fig. 4, refer to Fig S14-15 for other water year examples). With + 4°C warming across all seasons, water-limited conditions shift to higher elevations, and the East River becomes nearly snow-free. Sustained snowpack is concentrated only in the alpine and upper subalpine. Snowpack reductions and increased atmospheric demand drive soil moisture loss across all elevations but losses are greatest at the interface between the upper and lower subalpine where conifer density is highest. Soil moisture reductions are not substantial

above tree line where atmospheric demand remains less than precipitation and thin soils are largely reset even under these extremely dry and warm conditions. Despite large losses in snow accumulation, high elevation remnant snowpack is still able to support increased ET[56] but does so at the expense of downgradient interflow-derived streamflow and a net loss to recharge. Groundwater released from storage at lower elevations is also reduced in comparison to the historical condition (less negative, or DSg > 0). Despite this reduction in groundwater release, groundwater discharge maintains support of ET at the historical level at lower elevations (DET ~ 0) but is unable to sustain historical groundwater discharge to streams. Qg is reduced volumetrically by 20% with the largest reductions occurring in the montane. Summing Qs and Qg, total streamflow is reduced by 32% in the low precipitation water year example, with summer and fall temperatures responsible for two-thirds of this loss.

Groundwater storage declines amplify streamflow LOSS.

Groundwater storage aggregates climate over a 4-year period. Historically, this multi-year aggregation helps buffer extremely dry water years and promotes groundwater recovery back to the historical mean condition (Fig. 5a). Recently, however, the onset of low/no monsoon rain from 2016–2020 combined with the shock of an extremely dry water year in 2018, has prompted sustained declines in groundwater storage with losses simulated at greater than 2-standard deviations of the historical mean. This agrees with groundwater observations in the East River that indicate water table declines from 2018 are not recovering[57] (Fig. S16) despite above average snow accumulation in 2017, 2019 and 2022. Applying + 4°C warming to historical climate sequencing results in a groundwater system unable to recover to the historical average condition even during very wet periods simulated. The largest drops in storage occur after each exceptionally dry water year and losses exceed the historical low point after the first of these events. At the end of the hypothetical warming simulation, groundwater storage loss exceeds six standard deviations of the historical mean and does not appear to have stabilized. Results indicate summer temperature increase is responsible for the largest relative declines in groundwater storage and is nearly twice as influential on storage loss compared to spring warming with effects most pronounced during exceptionally dry years (Fig. S17).

Water table declines due to multi-decadal warming are nonuniformly distributed across the East River with changes largest in the subalpine (Fig. S18). Multiple linear regression analysis indicates high relief catchments covered by conifer forests are expected to experience the largest declines in groundwater storage in response to long-term warming (refer to Methods). Forests have higher rates of ET compared to non-woody vegetation[58] and will potentially out-compete for access of deeper water pools[59], while dense canopies are responsible for large interception losses to evaporation that are expected to increase in a warmer climate. These processes will reduce the downgradient transfer of interflow, recharge and result in lower water tables[60]. Extrapolating across the UCRB distinguishes regions most at risk of groundwater decline in a warmer future (Fig. 5b) and identifies possible areas for future forest management to increase groundwater sustainability[61]. Specifically, mountainous areas in the Colorado Headwater Basin and the Gunnison Basin are at elevated risk in a warmer future. Normalizing initial

subsurface storage conditions (refer to Methods), we find gradient-driven seepage loss results in 10–24% annual streamflow decline and 12–27% reductions in the 7-day minimum flow, with the influence of seepage loss on streamflow declines increasing at higher aridity (Fig. 6). Seepage loss is twice as effective at reducing annual streamflow compared to warming with no change in groundwater storage. Mitigation of temperature effects on annual streamflow declines occurs because sharp decreases in summer streamflow are largely offset by increased winter and early spring streamflow in response to earlier snowmelt that occurs when atmospheric demand and vegetation water use are low (Fig. 7). Seepage loss effects on summer flows are smaller but push the East River toward a dry riverbed during below average precipitation that are not predicted if the groundwater system is ignored.

summary

Mountain snowpack is a critical reservoir for downstream water use worldwide[62]. Dwindling supply is aggravating increased lowland demand in basins like the Colorado River, promoting political tensions and a need to better understand mechanisms of mountain discharge for better adaptive management. Hydrologic modeling studies have identified increased ET as a primary mechanism of streamflow reduction in a warmer climate, largely through decreased albedo with snow loss[12], but with spatial variability in response largely dictated by elevation[13]. While groundwater contributions are increasingly acknowledged as important to mountain streamflow, limited analysis has been done at the resolution for capturing recharge in complex terrain and linking to both snow and ET dynamics. We use a high-resolution, integrated hydrological model extended into the deep subsurface to determine if groundwater will buffer or amplify streamflow losses in a warmer world. Results for a representative headwater basin in the UCRB indicate that groundwater contributions have historically been a significant and stable contribution to stream water (26 ± 7%) and directly responsive to groundwater storage which aggregates climate over a 4-year period to minimize climate extremes. Groundwater sourcing occurs at higher elevations where precipitation inputs are in excess of atmospheric demand and discharges downgradient in water limited portions of the basin to support ET and stabilize groundwater sourcing to streams. Warming by + 4°C reduces snowpack, with snow accumulation largely confined to the highest elevations in the basin. Increased atmospheric demand and longer growing seasons promote more ET in the alpine and upper subalpine, while subsurface water subsidizes lower elevation ET at (or above) historic levels at the expense of interflow and groundwater discharge to streams. With warming, groundwater storage reductions exceed the historical minimum after the first extremely dry water year and are unable to recover to historical conditions even after multiple wet periods simulated. Given the cold and wet nature of this headwater basin, summer warming appears the most influential on groundwater storage loss through elevated ET and reduced soil moisture that adversely affects recharge in the subsequent snowmelt period. Resulting water table reductions promote increased seepage loss from streams to partially buffer recharge declines, but in doing so, significantly reduce annual streamflow, and forces minimum summer flow toward intermittent conditions that are not predicted if groundwater interactions are not considered. Water table declines are non-uniformly distributed. High relief catchments occupied by conifer forests are at particular risk. Results help identify those regions in the UCRB that may benefit

from the joint management of forest and water resources to minimize streamflow reductions in a warmer future. Our research stresses that including groundwater response to multi-decadal warming is necessary to forecast future response of mountain hydrology.

METHODS

Model Development

Hydrologic water budgets rely on the US Geological Survey (USGS) Groundwater and Surface water Flow model (GSFLOW)[37]. GSFLOW dynamically couples the USGS Precipitation-Runoff Modeling System[63] (PRMS) and the Newton formulation of the USGS three dimensional Modular Groundwater Flow Model[39] (MODFLOW). PRMS parameterization of the East River (ER) is described in previous work[64] but provided in brief for completeness. The data collection sites for model development are given in Fig. S1 with links to data provided in Table S1. USGS tools for GSFLOW input[65] helped parameterize elevation[66] and vegetation characteristics[35,67] of dominant cover type, summer and winter cover density, canopy interception characteristics for snow and rain, and transmission coefficients for short wave solar radiation. Climate for water years (wy is 1 Oct to 30 Sept) 1987 to 2022 was distributed using daily lapse rate of minimum and maximum temperature values from two snow telemetry stations (SNOTEL: Schofield site 737, and Butte site 380) and adjusted for aspect. Temperatures were bias corrected for sensor replacement[68] in the early 2000s. Shortwave solar radiation uses a degree-day method applicable for the Rocky Mountains[69] and calibrated to four weather stations operated by the Rocky Mountain Biological Laboratory (RMBL). Potential evapotranspiration (PET) was calculated using a modified version of the Jensen-Haise formation dependent on temperature and solar radiation[70]. Results were compared to a local eddy covariance flux station[71]. Observed daily precipitation at the Schofield SNOTEL was spatially distributed as either rain or snow based on a temperature threshold calibrated to match snow water equivalent (SWE) at the station. Snowfall distribution relied on airborne lidar maps of snow depth[33] converted to SWE based on ground surveys[72] and snow density modeling[73] conducted by ASO, inc. Parameterization used flight data for a wet water year near peak accumulation (7 April 2019) and adjusted for simulated losses associated with canopy interception, sublimation and early melt prior to the flight. Simulated SWE was validated using flight data collected during an average water year (4 April 2016) and two flights during a dry water year (30 March 2018, 24 May 2018) and snow depth at RMBL weather stations. Rainfall was distributed using the 30-year monthly Parameter-elevation Relationships on Independent Slopes Model[74]. Maximum soil water storage was estimated as the product of rooting depth[67] and available water content determined from soil type[75] and adjusted to match PRMS derived streamflow across the basin[64,76]. Additional PRMS parameter adjustment was done to match the furthest downstream gage (East at Almont, USGS 09112500) when fully coupled to MODFLOW. The Almont stream discharge Nash Sutcliffe Efficiency (NSE) = 0.81 and relative root mean squared error (rrmse) = 5% (log discharge NSE = 0.81, rrmse = 9%). Hydrographs for 15 stream gages are provided in Fig. S3-S4. Smaller catchments at higher elevation are simulated with rrmse ranging from 6–15% but tend toward

low NSE values (< 0.50). Error in estimating low-order daily streamflow is partly due to difficulty developing rating curves at these sites where shifting channel morphology and sensor malfunction/loss tended to occur with runoff and required rebuilding rating curves annually. USGS stations are simulated with rrmse less than 6% and NSE values tend toward values in excess of 0.8. Across all discharge stations, annual streamflow is simulated with 8% error.

A three-dimensional geologic model was developed for incorporation into the hydrological model to simulate subsurface processes over space and time. The geologic model was developed using Seequent's 3D Leapfrog geological modeling software which is based on implicit modeling using a radial basis function to generate surface discontinuities (e.g. horizons and faults) within the domain of interest[77–79]. The initial structural model was based on a series of USGS maps for the area at different scales (1:24k, 1:250k) which contained simplified geology to more complex structure with strike and dip, and fault throw information (Fig. S5). Maps of different geologic units were georeferenced and incorporated into Leapfrog and overlain on the digital elevation model. Structural discs were assigned to the boundaries where strike and dip information was observed on the geologic maps and fit to the published cross-sections. The horizon boundaries were digitized with polylines that captured the geologic structure. The structural model was then generated that honored the input data using the radial basis function.

Top and bottom information for each of the geologic units was extracted from Leapfrog as text files and processed for use in the hydrologic model. Specifically, eight geologic units are included in the groundwater model divided into six layers using a terrain-following grid approach with each layer of constant thickness for a total thickness of 400 m. The top model layer represents surface alluvium with spatial extent available from the 1:24K geologic maps. For regions in the model with information limited to the 1:150K geologic map, these surface units were inferred to occur along stream reaches. Geologic zones are identified within each layer using a zonal approach. The decay of hydraulic conductivity (K) with depth (Y) is defined using an exponential function $K = K_0 e^{(-A_0 Y)}$, with surface hydraulic conductivity (K_o) and a decay coefficient (A_o) calibrated to match observed groundwater water levels (Fig. S6, Table S2). K_o values align with previous catchment-scale groundwater models in the basin[43] and A_o = 0.05 is an acceptable value[80] that effectively maintains groundwater levels and perennial streams at high elevation while preventing flooding of the basin (Fig. S7-S8). Resulting perennial and non-perennial conditions match USGS classifications (Fig. S9). Water levels were found insensitive to geologic sub-zonal heterogeneity based on the statistical distribution of resistivity derived from an airborne electrical magnetic survey. The transient spin up was initiated with steady state water levels and run for 72 years (the historical climate period simulated twice) to stabilize unsaturated and saturated subsurface storage. Model simulations are organized in sequential 1-year increments with restart[81] files that are executed through a batch file. This approach allows model assessment and output management during execution and provides starting conditions for subsequent experiments assessing initial storage conditions.

Observed Climate Trends and Simulated Warming

Annual and season Schofield SNOTEL climate trend analysis applied linear least squares to assess historical seasonal change in the local area Table S3. Seasons defined as fall = September, October, and November, winter = December, January, and February, spring = March, April, and May, summer = June, July, and August. Mean, minimum and daily temperature prior to May 2003 applied bias correction[68] to account for senor replacement. Results indicate statistical significance in temperature increase across all seasons except spring, and maximum daily temperature is increasing faster than minimum daily temperature. Annually, the average daily temperature is increasing 0.44°C/decade. Seasonally, fall is experiencing the largest temperature increases at nearly double the annual rate. There has been no significant change in annual precipitation in the area, though a decrease in fall precipitation of nearly 10% per decade ($p < 0.05$) has occurred. Annual precipitation appears to follow a 12-year trend based on $P = Asin\left(wx + C\left(\frac{\pi}{180}\right)\right) + K$, where A = amplitude set to the historical annual standard deviation (175.8 mm/y), C = lag in years, K = SNOTEL historical mean (947.3 mm/y), and w = angular frequency. The lag and angular frequency were adjusted to minimize the sum squared error. Differences in means for each of the three 12-year cycles were tested using the independence of means t-test, and while the last cycle has lower annual and seasonal precipitation means, there are no statistical differences between cycles.

We assume + 4C warming to be representative of end-of-century and apply it both annually and to each season (fall, winter, spring, summer) independently across the historical climate sequencing. The approach is meant as a sensitivity analysis versus a replication of end of the century conditions. The experimental design allows a direct comparison to the historical baseline condition and a comparison of relative effects of season but does not account for incremental warming, seasonal variation in warming, non-uniform spatial response to temperature[82], the influence of the Clausius-Clapeyron relationship, or changes in extreme event sequencing[83]. Likewise, we do not simulate possible changes in vegetation water use response to elevated CO_2[84] or forest mortality[85,86].These will be addressed in future work.

Water Budget Analysis

Initial subsurface storage was set to the spin-up conditions obtained for 1 October 1987 to allow comparisons between different model runs. Annual water budgets averaged over the water year were done across all active model cells. Regressions are based on a least squared approach with the 99% confidence intervals provided (e.g. Fig. S9). Low monsoon conditions were defined as an annual rain anomaly, or z-score, less than − 0.5 which equates to annual rain less than 162 mm. Low monsoon rain is to have occurred water years 1989, 1996, 2002, 2004, 2008, 2011-12, 2016-17. A no-monsoon condition was defined as an annual rain anomaly less than − 1.0, or rain less than 133 mm and simulated to have occurred 1988, 1994, 2018–2020. Budyko[47] estimates were calculated as

$Y = (1 - \exp\left(-Xtanh\left(\frac{1}{X}\right)\right))^{0.5}$, where Y = PET/P, X = ET/P.

Annual deviation of groundwater storage from the historical average is assessed as a function of climate lag with a multiple linear regression. Climate variability is represented by annual aridity (PET/P). Aridity information for a given lag is kept in the multiple linear regression if the statistical significance of all independent variables is maintained ($p < 0.01$) and the coefficient of determination improves with added information. Results indicate that aridity with lag 0 (same year) has no predictive ability on simulated groundwater storage deviation ($r^2 = 0.05$, $p = 0.19$). Instead, groundwater storage deviation is best explained using four years of climate information that excludes lag 0 ($r^2 = 0.85$) with [GW Stor] = -3.1-66.5[X4] − 86.1[X3] − 106.6[X2] − 124.3[X 1]; with X4 = aridity lag 4 years ($p = 0.001$), X3 = aridity lag 3 years ($p = 7.5e-5$), X2 = aridity lag 2 years ($p = 2.7e-6$) and X1 = aridity lag 1 year ($p = 1.0e-7$). Daily cell-by-cell output for various water budget components are generated by PRMS in csv format and by MODFLOW in binary format. One-dimensional elevational plots aggregate simulated output across 50-m elevational increments. Aggregated values for the warming scenarios are then subtracted from the historical, or baseline, scenario (e.g. Figure 4). Sub-basins are defined by contributing area to either a stream gage for streamflow assessment, or by the USGS hydrographic unit code (HUC) level 12 catchment[87].

Changes in streamflow are divided into those associated with only temperature increase (DT), and those associated only with decreased subsurface storage (DS). Isolating effects was accomplished by selecting a range of historical water year climate inputs that span the full range of aridity simulated in the basin in order to capture historical variability in the timing of climate inputs (Fig. S19). Experimental design runs three simulations for each water year tested (i) Baseline: initial storage set to the 2016 historical condition with no change to historical climate input. (ii) Warming only: initial storage set to 2016 historical and + 4°C applied to climate input. (iii) Warming and Storage Loss: initial conditions set to 2016 given continuous warming and + 4°C applied to climate input. Storage loss effects isolated by subtracting (iii) from (ii) (Fig. S20). Initial conditions defined by 2016 chosen since historically its groundwater storage is near the historical average and under long-term warming it has significantly deviated from average (refer to Fig. 5a).

Upscaling Groundwater Risk to Warming

Multiple Linear Regression (MLR): Water table declines in the East River were calculated by subtracting water table elevations of the + 4°C warming from the historical period at the end of the multi-decadal simulation. Cell-by-cell differences were averaged across each of the ten HUC12 catchments in the East River. Water table declines were then regressed against a total of 35 climate and catchment characteristics. Climate characteristics of minimum and maximum temperature, minimum and maximum vapor pressure deficit, precipitation and solar radiation on a sloped surface use PRISM 30-year annual average (years 1991 to 2020). Table S1 identifies parameters and data sources used in the MLR. A python code was written to cycle through each combination of possible independent variables with the maximum number of independent variables kept less than or equal to four given the small sample size. For each iteration, the variable inflation factor (VIF) was calculated to assess multicollinearity between independent variables. The calculation regresses each independent variable (e.g. X1) with the other

independent variables (e.g. X2, X3, X4) and calculates the coefficient of determination with VIF(X1) = 1/(1-r^2) for each combination. MLR models containing a maximum VIF value greater than 5 are assumed to contain excessive multicollinearity and discarded. For acceptable models, the Akaike Information Criterion (AIC) is calculated. $AIC = 2k - \ln\left(\sum_{i=1}^{i=n}(O-P)^2\right)$, where *k* = number of predictor variables, O = average HUC12 water table decline estimated by GSFLOW, P = regression predicted water table decline. AIC accounts for covariance in predictor variables and limits redundancy of information in the regression analysis that can falsely inflate the strength of the regression. A lower value of AIC is considered a better model based on explanatory power and model simplicity. Model performance is evaluated using the leave one out cross validation (LOOCV) in which all data points except one are used to train the model and then tested on the single data point. The process is repeated for each data point. The mean squared error (MSE) in training observations are then averaged across all iterations for a given MLR model.

The best MLR model is assumed to contain the highest predictive power (r^2) while maintaining statistical significance ($p < 0.01$) of independent variables, with lower AIC and VIF considered for MLR models of equal predictive abilities. Of the 1.3 million possible combinations, 27,558 MRL models contained a VIF < 5 and 41 models had a coefficient of determination > 0.90. The best MLR model is defined as [dWT]= -7.13 + 1.48[TWI] + 0.0019[relief] + 3.81[fraction area grass] + 3.17[fraction area conifer] ($r^2 = 0.96$, $p = 0.004$). All independent variables are significant at $p \leq 0.002$. The dependent variable dWT is the change in water table elevation with dWT > 0 indicating the water table elevation becomes lower with warming. The topographic wetness index is a measure of potential moisture accumulation (TWI = ln(flow accumulation/(tan(slope) + 0.01)). It was calculated using ArcGIS Hydrology tools with a 30m DEM for fill, flow direction and accumulation. Slope is in radians. Higher values indicate locations where water is likely to collect based on topographic depressions or lower slope. The fraction of area that is conifer forest is the variable of largest predictive ability. Other metrics of evaluation include AIC = -12, maximum VIF = 3.25, LOOCV MSE = 0.03m.

Upscaling Approach: Mountainous catchments in the Upper Colorado River Basin (UCRB) are defined using a ruggedness metric where ruggedness is calculated as topographic relief across a focal averaging of roughly 7 km (231 30-m grid cells) applied across a rectangle about the point. Roughness values are then averaged for a given HUC12 catchment using zonal statistics in ArcGIS. A comparison with the GMCM v2[88] indicates close alignment for a roughness of approximately 400 m (Fig. S21). This equates to 1726 HUC12 catchments at 150,786 km^2, or 41% of the UCRB area. Independent variables for predicting change in groundwater elevation related to warming (TWI, relief, fgrass, fconifer) were calculated for all mountain catchments (Fig. S22-S25). The quartile method was applied to estimated UCRB water table declines. Groundwater risk is defined as low (< 0.72 m), moderate (0.72 to 1.58 m), high (1.58 to 2.24 m), and extreme (2.24 to 4.67 m). Limitations to the MLR include ignoring anthropogenic effects on groundwater storage from irrigation, groundwater pumping and reservoir storage. In addition, we assumed linear relationships between climate parameters and change in groundwater. This is a poor assumption and will need to be addressed in the future.

Declarations

Data Availability

Data description and source links are provided in Supplementary Table S1.xlxs. Metadata for Lawrence Berkeley National Laboratory Watershed Function Science Focus (SFA) field sites also provided here[89].

Code Availability and Model Files

The GSFLOW code version 2.0.0 is publicly available at https://www.usgs.gov/software/gsflow-coupled-groundwater-and-surface-water-flow-model with links provided for U.S. Geological Survey reports describing the code[37], developing GSFLOW input files[65], and restart simulations[81]. East River input files for the historical and warming simulations are provided at https://data.ess-dive.lbl.gov/datasets/doi:10.15485/1998576 with a readme.txt to guide model download and execution. The MLR python code, input file and output file are provided as supplementary data sets.

Acknowledgements

Work was supported by the US Department of Energy Office of Science under the contract DE-AC02-05CH11231. We thank Jeremy Snyder at LBNL for his help on Figure 7, and the Rocky Mountain Biological Laboratory for support on data collection and permitting.

Author contributions

RWHC designed the study, developed and ran the GSFLOW simulations, did the analysis, wrote the paper; RN provided invaluable support on GSFLOW model construction, reviewed model, output analysis and paper review; CU developed the geological model and assisted in its transfer to GSFLOW and helped in paper writing; CV assisted in upscaling analysis, data management and paper review; ESW advised on hypotheses, climate assessment, and paper review; KWH directed all field operations, assisted in study design, model analysis, figure review and paper writing.

References

1. Jacobs, J. Sustainability of Water Resources in the Colorado River Basin. *Bridge Link. Eng. Soc.* **41**, 6–12 (2011).
2. James, T., Madly, E. & Kelly, C. the Economic Importance of the Colorado River To the Basin Region. 1–54 (2014).
3. Udall, B. & Overpeck, J. he twenty-first century Colorado River hot drought and implications for the future. *Water Resour. Res.* **53**, 2404–2418 (2017).

4. Williams, A. P., Cook, B. I. & Smerdon, J. E. Rapid intensification of the emerging southwestern North American megadrought in 2020–2021. *Nat. Clim. Change* **12**, 232–234 (2022).
5. Wheeler, B. K. G. *et al.* What will it take to stabilize require difficult decisions to prevent further decline. 373–376 (2022).
6. Western Water Assessment. Water Year 2021 Summary. (2021) doi:https://wwa.colorado.edu/resources/intermountain-west-climate-dashboard/briefing/water-year-2021-summary.
7. Pepin, N. *et al.* Elevation-dependent warming in mountain regions of the world. *Nat. Clim. Change* **5**, 424–430 (2015).
8. Sexstone, G. A., Clow, D. W., Stannard, D. I. & Fassnacht, S. R. Comparison of methods for quantifying surface sublimation over seasonally snow-covered terrain. *Hydrol. Process.* **30**, 3373–3389 (2016).
9. Mote, P. W., Li, S., Lettenmaier, D. P., Xiao, M. & Engel, R. Dramatic declines in snowpack in the western US. *Npj Clim. Atmospheric Sci.* **1**, 2 (2018).
10. Huning, L. S. & AghaKouchak, A. Global snow drought hot spots and characteristics. *Proc. Natl. Acad. Sci.* 201915921 (2020) doi:10.1073/pnas.1915921117.
11. Siirila-Woodburn, E. R. *et al.* A low-to-no snow future and its impacts on water resources in the western United States. *Nat. Rev. Earth Environ.* **2**, 800–819 (2021).
12. Milly, P. C. D. & Dunne, K. A. Colorado River flow dwindles as warming-driven loss of reflective snow energizes evaporation. **9187**, 1–9 (2020).
13. Mastrotheodoros, T. *et al.* More green and less blue water in the Alps during warmer summers. *Nat. Clim. Change* **10**, 155–161 (2020).
14. Somers, L. D. & McKenzie, J. M. A review of groundwater in high mountain environments. *Wiley Interdiscip. Rev. Water* **7**, 1–27 (2020).
15. Beven, K. & Kierby, M. J. A physically-based, variable contributing area model of basin hydrology. *Hydrol. Sci. Bull.* **24**, 43–69 (1979).
16. Tetzlaff, D. *et al.* How does landscape sturcture influence catchment scale transit time across different geomorphic provinces? *Hydrol. Process.* **23**, 945–953 (2009).
17. Miller, M. P., Buto, S. G., Susong, D. D. & Rumsey, C. A. The importance of base flow in sustaining surface water flow in the Upper Colorado River Basin. *Water Resour. Res.* **52**, 3547–3562 (2016).
18. Rumsey, C. A., Miller, M. P., Susong, D. D., Tillman, F. D. & Anning, D. W. Regional Studies Regional scale estimates of baseflow and factors influencing baseflow in the Upper Colorado River Basin. *J. Hydrol.* **4**, 91–107 (2015).
19. Carroll, R. W. H. *et al.* Factors controlling seasonal groundwater and solute flux from snow-dominated basins. *Hydrol. Process.* **32**, 2187–2202 (2018).
20. Taylor, R. G. *et al.* Ground water and climate change. *Nat. Clim. Change* **3**, 322–329 (2012).
21. Huntington, J. L. & Niswonger, R. G. Role of surface-water and groundwater interactions on projected summertime streamflow in snow-dominated regions: an integrated modeling approach. *Water*

Resour. Res. **48**, (2012).

22. Engdahl, N. B. & Maxwell, R. M. Quantifying changes in age distributions and the hydrologic balance of a high-mountain watershed from climate induced variations in recharge. *J. Hydrol.* **522**, 152–162 (2015).
23. Deems, J. S., Fassnacht, S. R. & Elder, K. J. Fractal distribution of snow depth from LiDAR data. *J. Hydrometeorol.* **7**, 285–297 (2006).
24. Harpold, A. *et al.* Changes in snowpack accumulation and ablation in the intermountain west. *Water Resour. Res.* **48**, (2012).
25. Bales, R. *et al.* Mountain hydrology of the Western United States. *Water Resour. Res.* **42**, 1208 (2006).
26. Mott, R., Vionnet, V. & Grünewald, T. The Seasonal Snow Cover Dynamics: Review on Wind-Driven Coupling Processes. *Front. Earth Sci.* **6**, (2018).
27. Wang, K. & Dickinson, R. a Review of Global Terrestrial Evapotranspiration : Observation, Modeling, Climatology, and Climate Variability. *Rev. Geophys.* **50**, 1–54 (2012).
28. Meixner, T. *et al.* Implications of projected climate change for groundwater recharge in the western United States. *J. Hydrol.* **534**, 124–138 (2016).
29. Foster, L. M., Williams, K. H. & Maxwell, R. M. Resolution matters when modeling climate change in headwaters of the Colorado River. *Environ. Res. Lett.* **15**, (2020).
30. Varadharajan, C. *et al.* Challenges in Building an End-to-End System for Acquisition, Management, and Integration of Diverse Data from Sensor Networks in Watersheds: Lessons from a Mountainous Community Observatory in East River, Colorado. *IEEE Access* **7**, 182796–182813 (2019).
31. Battaglin, W., Hay, L. & Markstrom, S. Simulating the potential effects of climate change in two Colorado basins and at two Colorado ski areas. *Earth Interact.* **15**, 1–23 (2011).
32. Hubbard, S. S. *et al.* The East River, Colorado, watershed: A mountainous community testbed for improving predictive understanding of multiscale hydrological–biogeochemical dynamics. *Vadose Zone J.* **17**, (2018).
33. Painter, T. H. *et al.* The Airborne Snow Observatory: Fusion of scanning lidar, imaging spectrometer, and physically-based modeling for mapping snow water equivalent and snow albedo. *Remote Sens. Environ.* **184**, 139–152 (2016).
34. ASO Inc. Airborne Snow Observatory, Inc. lidar derived snow depths and snow water equivalent. (2023) doi:https://data.airbornesnowobservatories.com/.
35. Breckheimer, I. High resolution landcover maps for the upper Gunnison Basin derived from LiDAR and NAIP imagery. *Watershed Funct. Sci. Focus Area* (2021).
36. Uhlemann, S. *et al.* Surface parameters and bedrock properties covary across a mountainous watershed: Insights from machine learning and geophysics. *Sci. Adv.* **8**, 1–16 (2022).
37. Markstrom, S. L., Niswonger, R. G., Regan, R. S., Prudic, D. E. & Barlow, P. M. GSFLOW – Coupled Ground-Water and Surface-Water Flow Model Based on the Integration of the Precipitation-Runoff

Modeling System (PRMS) and the Modular Ground-Water Flow Model (MODFLOW-2005): *US Geol. Surv. Tech. Methods* **6-D1**, 240 (2008).

38. Carroll, R. W. H. *et al.* Modeling Snow Dynamics and Stable Water Isotopes Across Mountain Landscapes. *Geophys. Res. Lett.* **49**, 1–10 (2022).
39. Niswonger, R. G., Panday, S. & Ibaraki, M. MODFLOW-NWT, a Newton formualtion for MODFLOW-2005. *US Geol. Surv. Tech. Methods* **6-A37**, 44 p. (2011).
40. Niswonger, R. G. & Prudic, D. E. Documentation of the Streamflow-Routing (SFR2) Package to include unsaturated flow beneath streams - a modification to SFR1. *US Geol. Surv. Tech. Methods* **6-A13**, 50 p. (2005).
41. Gaskill, D. L., Mutschler, F. E., Kramer, J. H., Thomas, J. A. & Zahony, S. G. Geologic map of the Gothic Quadrangle, Gunnison County, Colorado. (1991).
42. Condon, L. E. *et al.* Where Is the Bottom of a Watershed? *Water Resour. Res.* **56**, 0–3 (2020).
43. Carroll, R. W. H., Manning, A. H., Niswonger, R., Marchetti, D. & Williams, K. H. Baseflow Age Distributions and Depth of Active Groundwater Flow in a Snow-Dominated Mountain Headwater Basin. *Water Resour. Res.* **56**, 1–19 (2020).
44. Frisbee, M. D., Tolley, D. G. & Wilson, J. L. Field estimates of groundwater circulation depths in two mountainous watersheds in the western U.S. and the effect of deep circulation on solute concentrations in streamflow. *Water Resour. Res.* **53**, 2693–2715 (2017).
45. Carroll, R. W. H., Gochis, D. & Williams, K. H. Efficiency of the Summer Monsoon in Generating Streamflow Within a Snow-Dominated Headwater Basin of the Colorado River. *Geophys. Res. Lett.* **47**, (2020).
46. Ryken, A. C., Gochis, D. & Maxwell, R. M. Unravelling groundwater contributions to evapotranspiration and constraining water fluxes in a high-elevation catchment. *Hydrol. Process.* **36**, e14449 (2022).
47. Budyko, M. I. *Climate and Life*. (Elsevier, 1974).
48. Hahm, W. J. & Dralle, D. N. Low Subsurface Water Storage Capacity Relative to Annual Rainfall Decouples Mediterranean Plant Productivity and Water Use From Rainfall Variability Geophysical Research Letters. 6544–6553 (2019) doi:10.1029/2019GL083294.
49. McNamara, J. P., Chandler, D., Seyfried, M. & Achet, S. Soil moisture states, lateral flow, and streamflow generation in a semi-arid, snowmelt-driven catchment. *Hydrol. Process.* **19**, 4023–4038 (2005).
50. Anderson, M. G. & Burt, T. P. The role of topography in controlling throughflow generation. *Earth Surf. Process. Landf.* **3**, 331–344 (1978).
51. Carroll, R. W. H., Deems, J. S., Niswonger, R., Schumer, R. & Williams, K. H. The Importance of Interflow to Groundwater Recharge in a Snowmelt-Dominated Headwater Basin. *Geophys. Res. Lett.* **46**, 5899–5908 (2019).
52. Carroll, R. W. H., Deems, J. S., Niswonger, R., Schumer, R. & Williams, K. H. The Importance of Interflow to Groundwater Recharge in a Snowmelt-Dominated Headwater Basin. *Geophys. Res. Lett.*

46, 5899–5908 (2019).

53. Perdrial, J. N. *et al.* Stream water carbon controls in seasonally snow-covered mountain catchments: impact of inter-annual variability of water fluxes, catchment aspect and seasonal processes. *Biogeochemistry* **118**, 273–290 (2014).
54. Swetnam, T. L., Brooks, P. D., Barnard, H. R., Harpold, A. A. & Gallo, E. L. Topographically driven differences in energy and water constrain climatic control on forest carbon sequestration. *Ecosphere* **8**, (2017).
55. Hwang, T., Band, L. E., Vose, J. M. & Tague, C. Ecosystem processes at the watershed scale: Hydrologic vegetation gradient as an indicator for lateral hydrologic connectivity of headwater catchments. *Water Resour. Res.* **48**, 1–16 (2012).
56. Rumpf, S. B. *et al.* From white to green: Snow cover loss and increased vegetation productivity in the European Alps. *Science* **376**, 1119–1122 (2022).
57. Faybishenko, B. *et al.* QA/QC-ed Groundwater Level Time Series in PLM-1 and PLM-6 Monitoring Wells, East River, Colorado (2016-2022). (2023) doi:10.15485/1866836.
58. Zhang, L., Dawes, W. R. & Walker, G. R. Response of mean annual evapotranspiration to vegetation changes at catchment scale. *Water Resour. Res.* **37**, 701–708 (2001).
59. Mollnau, C., Newton, M. & Stringham, T. Soil water dynamics and water use in a western juniper (Juniperus occidentalis) woodland. *J. Arid Environ.* **102**, 117–126 (2014).
60. Carroll, R. W. H. *et al.* Evaluating mountain meadow groundwater response to Pinyon-Juniper and temperature in a great basin watershed. *Ecohydrology* **10**, e1792 (2017).
61. Smerdon, B. D., Redding, T. & Beckers, J. An overview of the effects of forest management on groundwater hydrology. *J. Ecosyst. Manag.* (2009) doi:10.22230/jem.2009v10n1a409.
62. Viviroli, D. & Weingartner, R. Water Towers"—A Global View of the Hydrological Importance of Mountains. in *Mountains: Sources of Water, Sources of Knowledge* (ed. Wiegandt) 15–20 (Springer, 2008).
63. Markstrom, S. L. *et al.* PRMS-IV, the precipitation-runoff modeling system, version 4. *US Geol. Surv. Tech. Methods Book 6 Chap B7* 158 (2015) doi:http://dx.doi.org/10.3133/tm6B7.
64. Carroll, R. W. H. *et al.* Variability in observed stable water isotopes in snowpack across a mountainous watershed in Colorado. *Hydrol. Process.* **36**, (2022).
65. Gardner, M. A., Morton, C. G., Huntington, J. L., Niswonger, R. G. & Henson, W. R. Input data processing tools for the integrated hydrologic model GSFLOW. *Environ. Model. Softw.* **109**, 41–53 (2018).
66. U.S. Geological Survey. National Elevation Dataset (NED). (2019).
67. LANDFIRE. Existing vegetation type and cover layers. *U.S. Department of the Interior, Geological Survey* http://landfire.cr.usgs.gov/viewer/(accessed May 2017) (2015).
68. Oyler, J. W., Dobrowski, S. Z., Ballantyne, A. P., Klene, A. E. & Running, S. W. Artificial amplification of warming trends across the mountains of the western United States. *Geophys. Res. Lett.* **42**, 153–161

(2015).

69. Leavesley, G. H., Markstrom, S. L., Brewer, M. S. & Viger, R. J. The Modular Modeling System (MMS)—The physical process modeling component of a database-centered decision support system for water and power management. *Water. Air. Soil Pollut.* **90**, 303–3011 (1983).
70. Jensen, M. E., Rob, D. C. N. & Franzoy, C. E. Scheduling irrigations using climate-crop-soil data. in *National Conference on Water Resources Engineering of the American Society of Civil Engineers* 20 p. (1969).
71. Ryken, A. C., Gochis, D. & Maxwell, R. M. Unravelling groundwater contributions to evapotranspiration and constraining water fluxes in a high-elevation catchment. *Hydrol. Process.* **36**, (2022).
72. Carroll, R., Brown, W., Newman, A., Buetler, C. & Williams, K. H. East River Watershed Stable Water Isotope Data in Precipitation, Snowpack and Snowmelt 2016-2020. *ESS-DIVE* (2021) doi:https://data.ess-dive.lbl.gov/view/doi:10.15485/1824223.
73. Marks, D., Domingo, J., Susong, D., Link, T. & Green, D. A spatially distributed energy balance snowmelt model for application in mountain basins. *Hydrol. Process.* **13**, 1935–1959 (1999).
74. OSU. *PRISM Climate Group*. http://prism.oregonstate.edu (2012).
75. NRCS. Web Soil Survey. *United States Department of Agriculture* http://websoilsurvey.nrcs.usda.gov/accessed March 2016 (1991).
76. Carroll, R. W. H. & Williams, K. H. Discharge data collected within the East River for the Lawrence Berkeley National Laboratory Watershed Function Science Focus Area (Water years 2015-2018). *ESS-DIVE* (2019) doi:http://dx.doi.org/10.21952/WTR/1465929.
77. Godwin, L., Valleau, N. & Mortimer, D. The evolution of geoscientific software–The past, present and future. in 135–136 (Society of Exploration Geophysicists and Environment and Engineering Geophysical Society, 2021).
78. Cowan, E. J., Beatson, R. K., Fright, W. R., McLeenan, T. J. & Mitchell, T. J. Rapid geological modelling. in 23–25 (2002).
79. Alcaraz, S. *et al.* 3d geological modelling using new Leapfrog Geothermal software. in *Proceedings of the 36th Workshop on Geothermal Reservoir Engineering* vol. 31 (2011).
80. Jiang, X.-W., Wan, L., Wang, X.-S., Ge, S. & Liu, J. Effect of exponential decay in hydraulic conductivity with depth on regional groundwater flow. *Geophys. Res. Lett.* **36**, (2009).
81. Regan, R. S., Niswonger, R. G., Markstrom, S. L. & Barlow, P. M. Documentation of the restart option for the U.S. Geological Survey coupled groudnwater and surface-water flow (GSFLOW) model. *US Geol. Surv. Tech. Methods* **6-D3**, (2015).
82. Faybishenko, B., Arora, B., Dwivedi, D. & Brodie, E. Statistical framework to assess long-term spatio-temporal climate changes: East River mountainous watershed case study. *Stoch. Environ. Res. Risk Assess.* **37**, 1303–1319 (2023).
83. Ombadi, M., Risser, M. D., Rhoades, A. M. & Varadharajan, C. A warming-induced reduction in snow fraction amplifies rainfall extremes. *Nature* **619**, 305–310 (2023).

84. Swann, A. L. S., Hoffman, F. M., Koven, C. D. & Randerson, J. T. Plant responses to increasing CO_2 reduce estimates of climate impacts on drought severity. *Proc. Natl. Acad. Sci.* **113**, 10019–10024 (2016).
85. Bearup, L. a, Maxwell, R. M., Clow, D. W. & Mccray, J. E. Hydrological effects of forest transpiration loss in bark beetle-impacted watersheds. *Nat. Clim. Change* **4**, 481–486 (2014).
86. Williams, P. A. *et al.* Temperature as a potent driver of regional forest drought stress and tree mortality. *Nat. Clim. Change* **3**, 292–297 (2012).
87. U.S. Geological Survey. National Hydrography Dataset (NHD) for Hydrologic Unit Code (HUC)-12. (2013).
88. Snethlage, M. A. *et al.* A hierarchical inventory of the world's mountains for global comparative mountain science. *Sci. Data* **9**, 149 (2022).
89. Varadharajan, C. *et al.* Location Identifiers, Metadata, and Map for Field Measurements at the East River Watershed, Colorado, USA (Version 3.0). (2022) doi:10.15485/1660962.

Figures

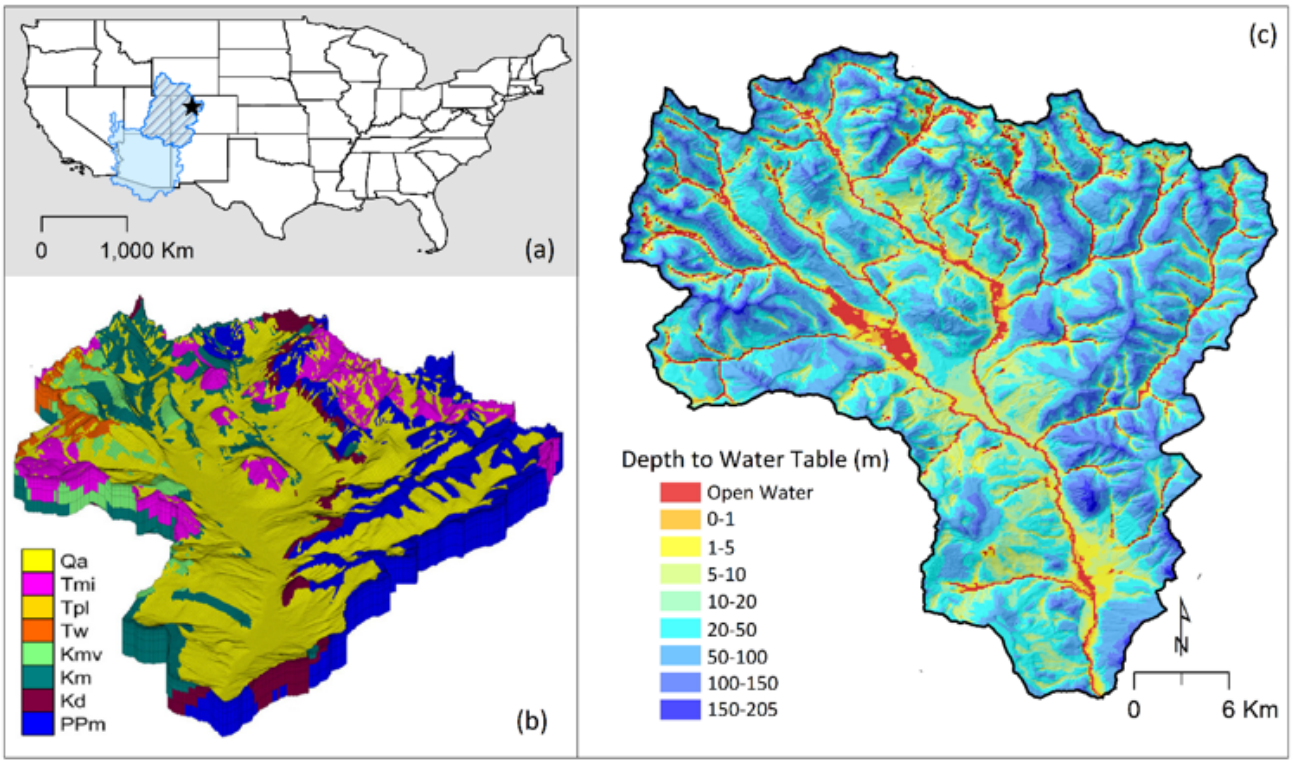

Figure 1

Simulating groundwater at high spatial resolution and to depth (400 m) in the headwaters of the Colorado River. (a) the East River (black star, 750 km^2) in the Colorado River Basin (blue shading) in the southwest United States. The Upper Colorado River Basin (UCRB) is shown in striped shading. (b)

Geologic model representing Tertiary igneous intrusive (Tmi), Permian, Cretaceous and Tertiary sandstones (PPm, Kd, Tw) Cretaceous mudstone (Kmv), Cretaceous shale (Km) and Quaternary alluvium (Qa). Description of geologic units provided in Table S2. (c) Simulated steady state depth to groundwater at the 100-m resolution with open water indicative of groundwater-fed, perennial streamflow, and inundated floodplains.

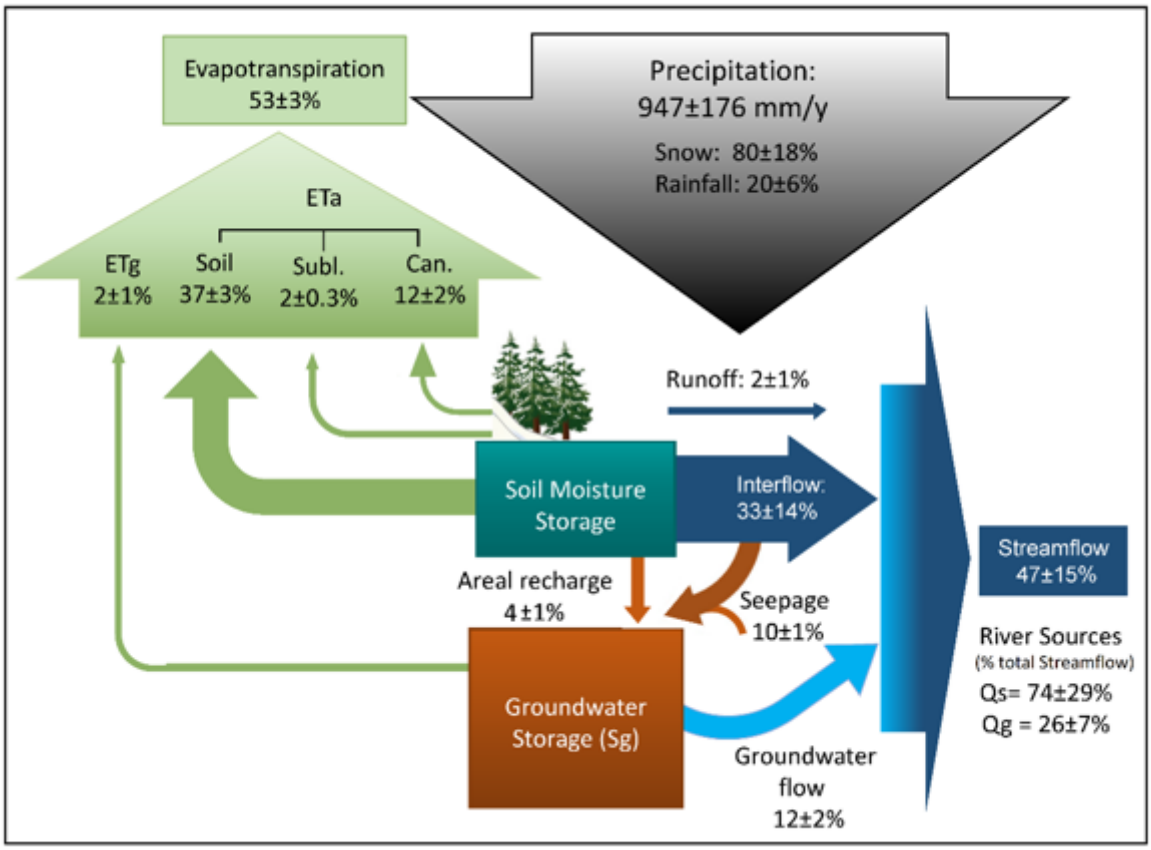

Figure 2

Historical basin-scale water budget averaged over water years 1987 to 2022. Results illustrate (i) that evapotranspiration (ET) is a dominant use of precipitation despite being a wet and cold basin, (ii) interflow is highly variable as a function of interannual climate (refer to Fig. S10d), and (iii) groundwater is a significant and relatively stable source of streamflow. Average annual water fluxes and standard deviations are presented as a percentage of average annual precipitation across different hydrologic subcomponents to determine river sources (Qs = interflow + runoff; Qg = groundwater). ET is the combined effect of groundwater ET (ETg), soil ET, Sublimation (Subl.) and canopy interception (Can.). Arrow size reflects relative flux volume.

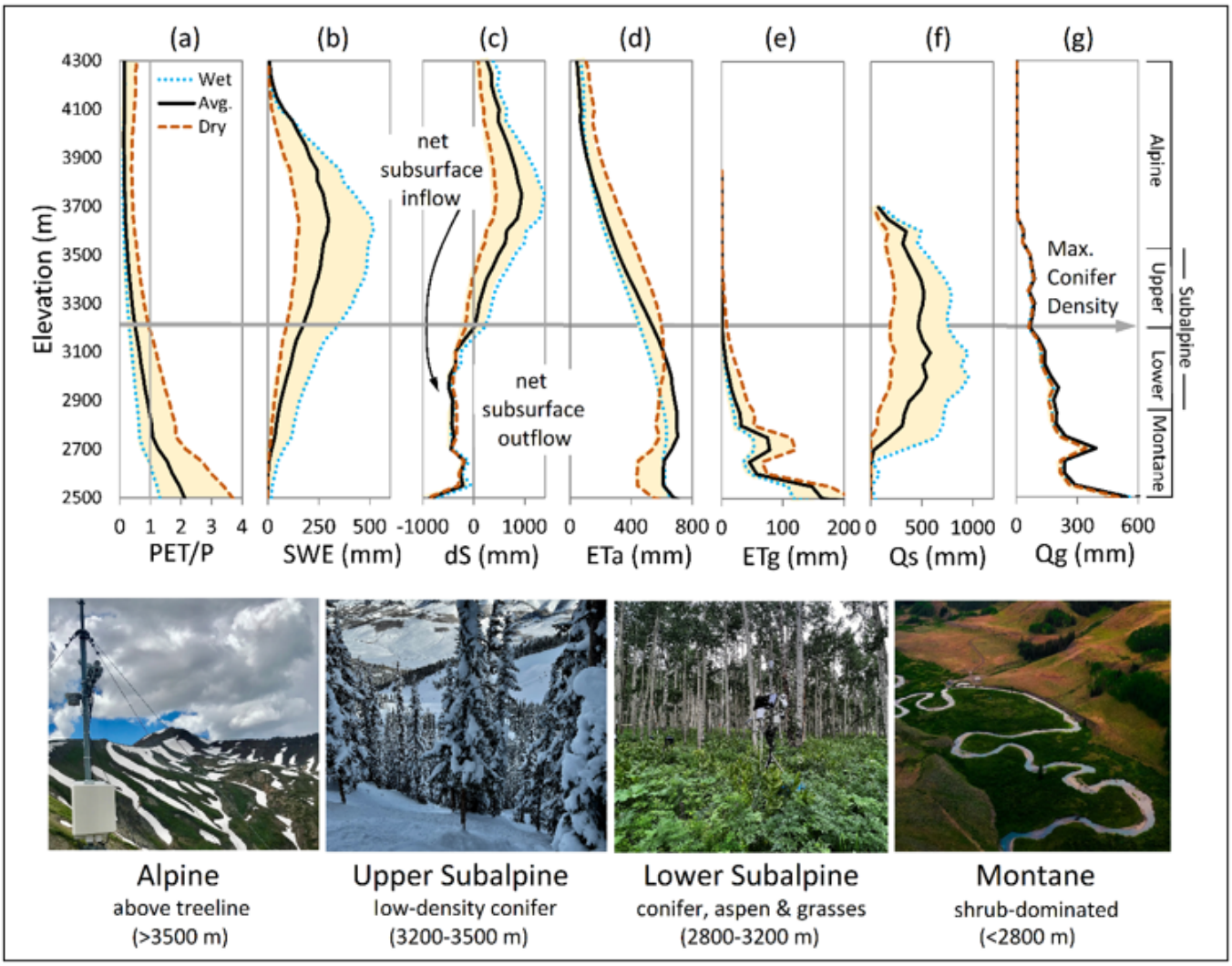

Figure 3

Elevation is a first-order control on climate, vegetation, and hydrology with the subsurface transfer of snowmelt subsidizing evapotranspiration and stream water. Averaged water budget terms across elevation for a historically wet, average, and dry water year: (a) aridity, PET/P, (b) average snow water equivalent, SWE. (c) change in subsurface storage, dS (d) ET excluding groundwater ET, or ETa (e) groundwater ET, ETg, (f) surface runoff plus interflow to streams, Qs, and (g) groundwater flow to streams, Qg. Vegetation zones are alpine, upper subalpine, lower subalpine and montane with the montane floodplains containing shallow depth to water and inundation during spring melt. dS = P-ET-Q; dS>0 subsurface inflow, dS<0 subsurface outflow.

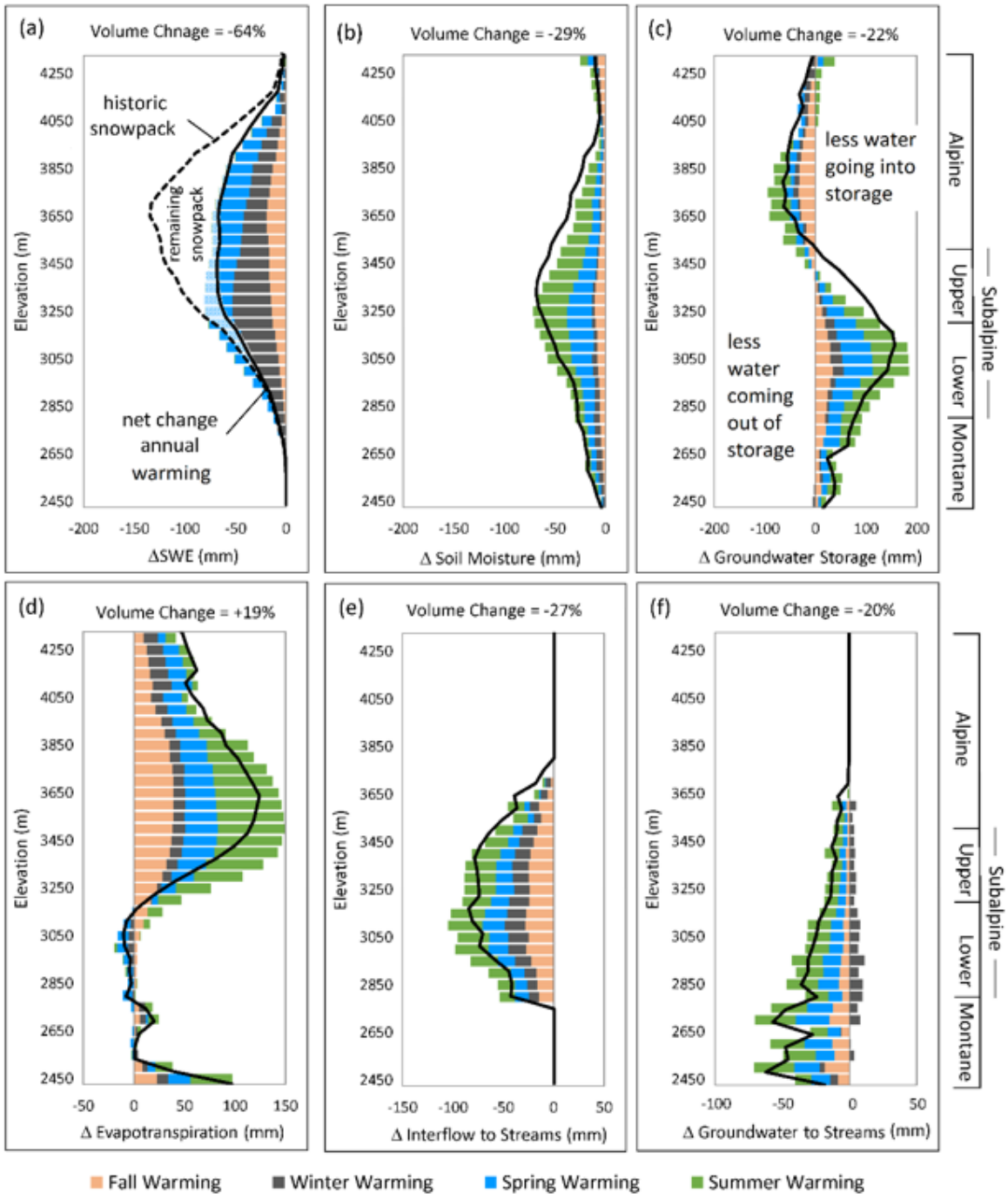

Figure 4

Cascading hydrologic effects of +4°C warming on streamflow loss for a dry water year across elevation. Annual change (D) defined as warming scenario minus historical condition (D<0 a reduction with warming). Water storage changes: (a) Snow water equivalent, SWE with historic snowpack provided to illustrate remaining snowpack with warming, (b) soil moisture, (c) annual groundwater storage. Water flux changes: (d) evapotranspiration (e) interflow to streams, (f) groundwater to streams. No streams

simulated >3650 m. Solid black line is the effect of warming applied to all seasons, or annually. Seasonal warming done independently does not sum to warming across all seasons due to seasonal memory. For example, snow melted in the winter cannot be melted in the spring in the annual warming scenario but can in the spring-only warming scenario. The effect is that annual warming tends to predict smaller hydrologic changes compared to the sum of seasonal warming, and a tendency for a slight shift in response toward higher elevations. Fall = September, October, November; Winter = December, January, February; Spring = March, April, May; Summer = June, July, August. Total volume change accounts for contributing area. Ecozones are indicated across elevation.

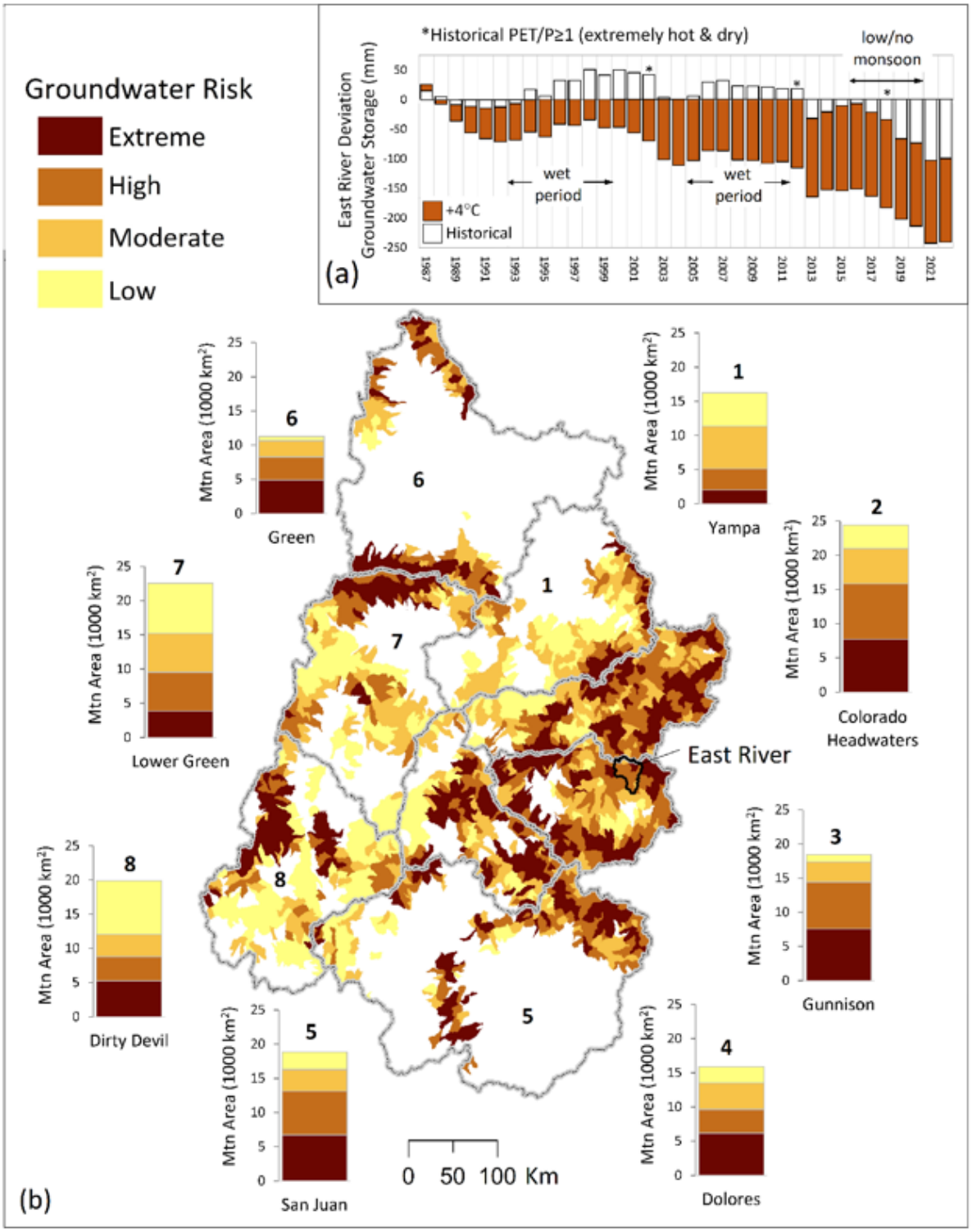

Figure 5

Groundwater storage loss in the East River is predicted to not rebound to historical conditions even during significant wet periods, with predicted storage loss non-uniformly distributed across the Upper Colorado River Basin. (a) Simulated East River average annual groundwater storage deviation from the historical average condition for both the historical and +4C warming scenarios. Wet periods and historically dry and warm years marked. Note the average historical condition has a deviation in groundwater storage = 0,

while deviation <0 indicates a decline from average and >0 indicates an increase above average. (b) Regional assessment of groundwater risk for mountainous catchments in the Upper Colorado River Basin due to muti-decadal warming. Results indicate the Colorado Headwaters (2) and the Gunnison (3) HUC4-level basins are most at risk of high or extreme water table declines. The location of the East River in the Gunnison Basin provided. The location of the UCRB with respect to the western US is provided in Fig. 1.

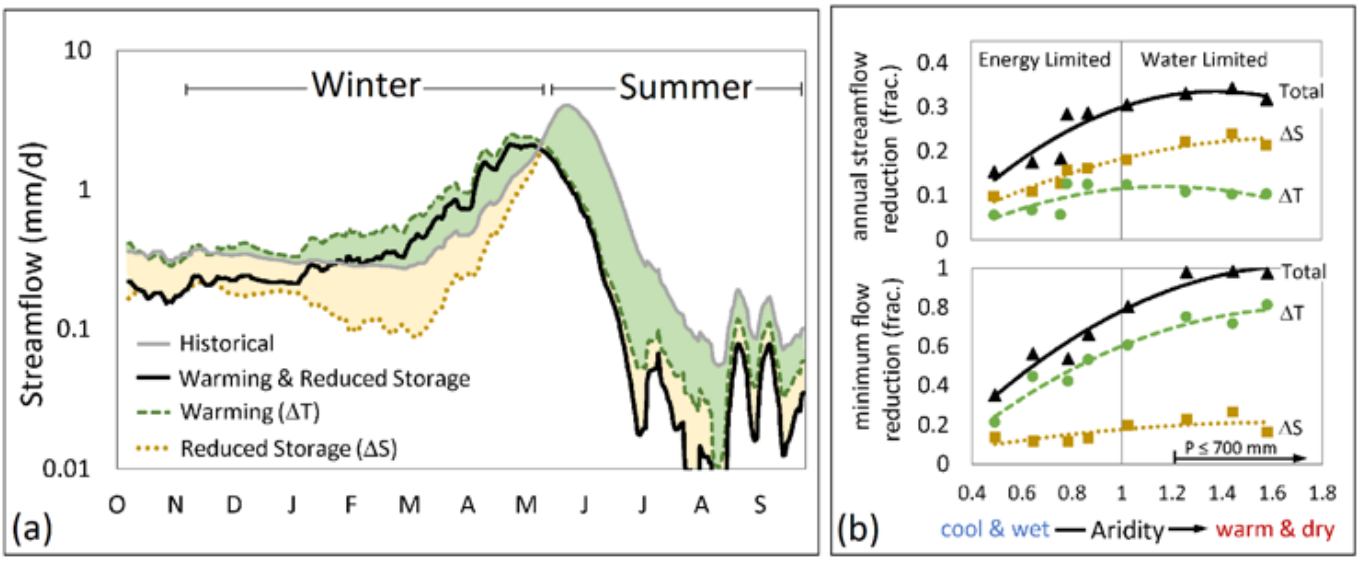

Figure 6

Long-term warming and associated water table declines will affect seasonal streamflow with significantly reduced annual average and minimum flows. Reductions in streamflow will be largest when precipitation inputs are low. Winter is broadly characterized as relatively low atmospheric demand and vegetation water use while summer is high atmospheric demand and water use. (a) Effects of reduced groundwater storage (DS, yellow shading) and temperature increase (DT, green shading) on a low precipitation water year hydrograph with the total effect of both (black line) and comparisons made to historical conditions (gray line). (b) Change from the historical condition for annual streamflow and the 7-day minimum flow across an aridity gradient (PET/P). The East River becomes non-perennial in the late summer (fraction of flow reduction approaches 1) when precipitation P≤700 mm and including groundwater storage declines in the estimate.

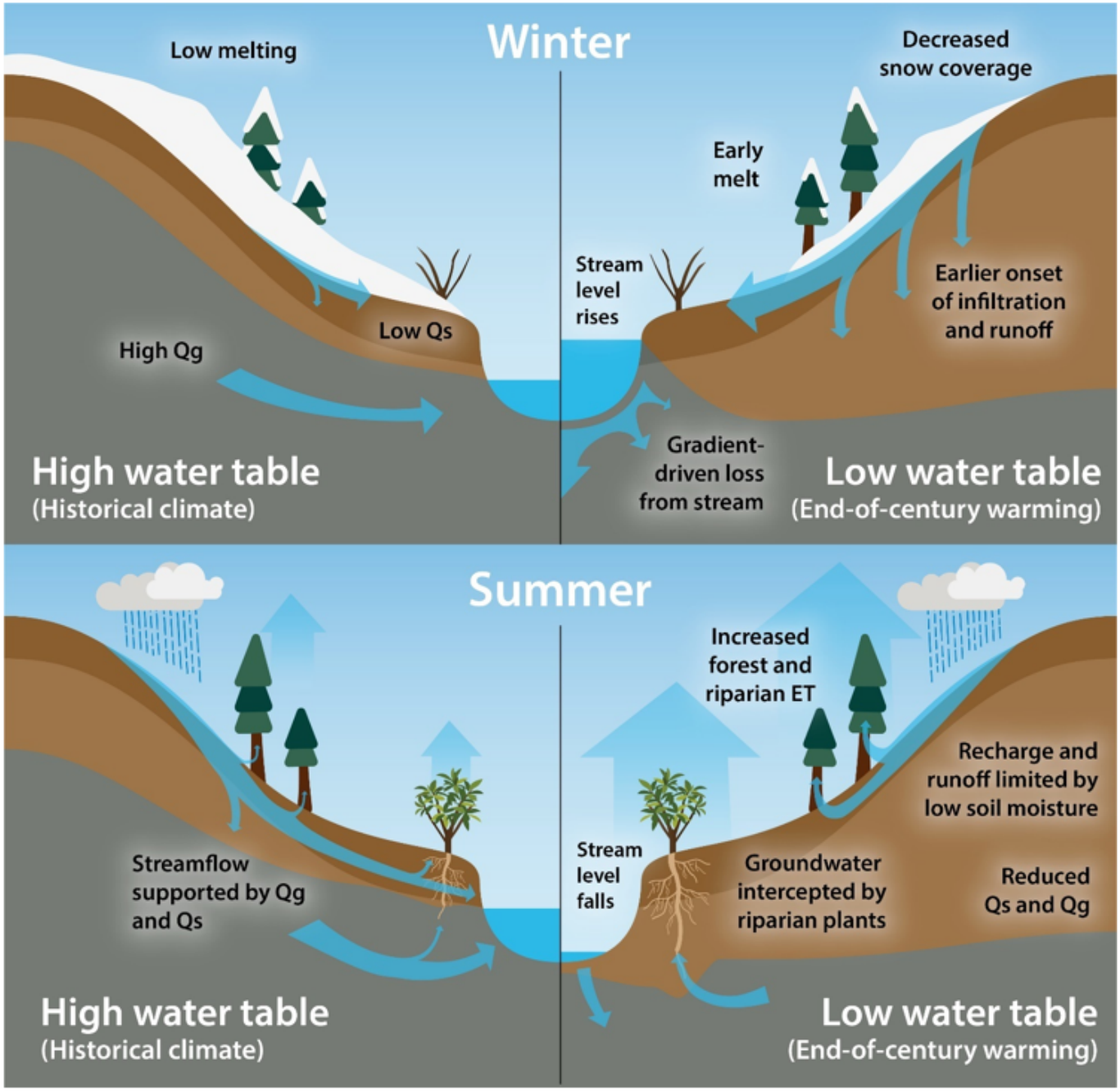

Figure 7

A warmer climate and lowered water table elevations will shift a greater fraction of stream water into the subsurface through gradient-driven loss. *Winter effects*: warming will decrease snow coverage and promote earlier onset of infiltration and runoff, though the net effect of annual recharge will be less than under historical conditions. Increased winter stream stage coupled with lower water table elevations will drive increased streamflow loss. *Summer effects*: Higher temperatures will promote increased evapotranspiration in the forested areas (and riparian zones) to limit lateral movement of subsurface flow into stream channels. Streams disconnected from the groundwater system through falling water

tables will become losing. Summer streamflow will be significantly lower with a possible transition toward non-perennial conditions.

Supplementary Files

This is a list of supplementary files associated with this preprint. Click to download.

- TableS1.xlsx
- MLRbuild.txt
- traits.csv
- iterationresults.csv
- rcarrollNatWatSI.pdf